

# Scarring in vibrational modes of thin metal plates

Andre J. Starobin and Stephen W. Teitsworth

*Duke University, Department of Physics, Box 90305, Durham, NC 27708-0305*

(November 15, 2018)

## Abstract

We report the first direct experimental observation of scarring phenomenon in transverse vibrational modes of a thin metal plate. The plate has the shape of a full stadium and clamped boundary conditions. Normal modes are imaged using time-averaged holographic interferometry, and modes corresponding to “bouncing ball” and higher order periodic trajectories are found. An eikonal approximation of the solution along classical trajectories of the stadium including nontrivial phase shifts at clamped boundaries yields a useful quantization condition for the observed modes.

PACS numbers: 05.45.Mt, 03.65.Sq, 46.40.-f

arXiv:nlin/0010028v2 [nlin.CD] 3 Dec 2001

Scarring refers to the build-up of amplitude along unstable periodic trajectories in high order modes of certain wave systems. The term is generally reserved for wave problems with domains which correspond to classically chaotic billiards. The phenomenon was first reported in numerical studies of high order, short wavelength modes of the Helmholtz equation inside a domain known as the Bunimovich stadium [1]; an explanation of scarring relies on methods of quantum chaos [1,2]. The Helmholtz equation serves, for example, as the time-independent Schrödinger equation for a particle in a box, and also as the equation governing the transverse vibration of elastic membranes. In addition to numerical studies of the Helmholtz equation, several analogue experiments have reported quantum chaotic spectral and spatial properties including the electromagnetic field modes of quasi-two-dimensional microwave cavities [3-5], stationary capillary waves on water [6], three-dimensional acoustic resonances in water-filled cavities [7], and vibrational modes of drumheads [8].

A possible extension of quantum chaos methods to the high frequency limit of wave problems with modes that are not described by the Helmholtz equation was noted by Berry [9]. The statistical properties of spectra as predicted by random matrix theory have since been confirmed in experiments on elastic waves in three-dimensional metal blocks [10-13], and on studies of electromagnetic modes in three-dimensional microwave cavities [14,15]. In both of these cases the vectorial nature of the modes destroys the exact analogy with the time-independent Schrödinger equation. More recently, scar-like phenomena have been reported for the electromagnetic modes of three-dimensional microwave cavities, although the role of underlying periodic orbits is unclear [16].

The transverse vibrational waves of a thin plate provide another important example of a wave system for which the stationary modes are not described by the Helmholtz equation. In a recent numerical study [17], the computed asymptotic spectrum for a fully clamped thin plate was shown to possess statistical properties predicted by random matrix theory; furthermore, the authors found strong evidence of scarring in vibrational amplitude plots for some of the high frequency modes. More recently, a general theory of scarring and spectral properties has been developed by Bogomolny and Hughes for transverse vibrations in thin plates [18]. In this paper, we present experimental results on the high frequency properties of vibrating metal plates, with particular attention given to the distinguishing spatial properties of individual high order modes. To our knowledge, this is the first report of scarring phenomena in an experimental vibrating plate. We also present a quantization criterion for the eigenfrequencies of modes that are scarred by particular classical periodic orbits. This criterion includes the effects of angle-dependent phase shifts associated with reflection of periodic orbits at the fully clamped boundary of a thin plate.

For our experiment, we have studied a stainless steel plate of thickness  $h = 0.305$  mm. The plate is in the shape of a full stadium and consists of a square central section of side 8.00 cm and two semi-disks on each side of radius  $R = 4.00$  cm. Contour plots of vibrational amplitude for individual modes are obtained using the technique of time-averaged holographic interferometry [19]. Characteristic vibrational amplitudes are of the same order as the wavelength of the 1 mW frequency-stabilized HeNe laser used for imaging. To achieve a fully clamped boundary condition (i.e., both amplitude and its normal derivative tend to zero at the boundary), the plate edges were carefully epoxied to a massive aluminum support. The interferograms of all imaged modes show that the vibrational amplitudes and amplitude gradients at the boundary are very small, thus confirming the effectiveness of the clamping

procedure. To drive the plate vibrations harmonically, we use a modified audio speaker (frequency range from 50 Hz to 12 kHz) which is coupled to the plate via a thin steel rod which acts as the driving rod. The rod is firmly attached to the speaker voice coil at one end and lightly epoxied to the plate at the other end. A scannable phonograph cartridge stylus is used to monitor the amplitude response of the plate at various positions. The signal is filtered through a low-noise pre-amplifier before being fed to an HP 3561A signal analyzer which is used to measure the resonant frequency and quality factor ( $Q$ ) for each detectable mode. Significant damping due to coupling of the plate to the support structure and the driving rod sets in at approximately 12 kHz, at which point the quality factors of the system become too low to resolve individual modes. The fundamental frequency of the plate is approximately 200 Hz.

In the frequency range between seven and eight kilohertz we find four vibrational resonances at  $7272\text{Hz}$ ,  $7442\text{Hz}$ ,  $7622\text{Hz}$  and at  $7874\text{Hz}$ . The wave patterns excited at  $7442\text{Hz}$  and at  $7622\text{Hz}$  reveal prominent scarring in the imaged amplitude distributions. Figure 1a shows the holographic interferogram, effectively an amplitude contour plot, for the  $7442\text{Hz}$  frequency of excitation. The large, connected bright areas correspond to places with very small vibrational amplitude, while darker areas and their interiors correspond to regions with large amplitude. Clearly visible in Fig. 1a is scarring by a “bouncing ball” trajectory across the width of the stadium plate; furthermore, we can see that there are 7 antinode pairs as one traverses the complete periodic trajectory. The excited wave pattern has a broken symmetry with respect to  $\beta$  symmetry axis of the plate, with the symmetry axis of the plate and the position of the driving rod-to-plate contact designated in Figure 1b. The symmetry with respect to  $\alpha$  axis is partially preserved on the left side of the plate. Further, while the left side of the plate displays a clear build-up of amplitude along the “bouncing ball” orbit and has regular radial amplitude features in left semi-disk, features characteristic of the (6,3) modes of a pure disk, the amplitude distribution in the right half of the plate does not appear regular and does not show any obvious scarring.

Figure 2 shows the interferogram for the  $7622\text{Hz}$  mode. In this case, scarring on the right side of the plate clearly follows a rectangular orbit producing a “whispering gallery” type mode. The number of antinodes traversed in going around the right half of the orbit is 16, which suggests that the total number of antinode pairs for the full orbit is 16. This resonant wave pattern is almost perfectly localized on the right-hand side of the plate, the same side where the speaker rod is glued to the plate. The semi-rectangular scar feature is confined fully to the right half of the plate and is essentially symmetric with respect to the  $\alpha$  axis. Immediately to the left of the  $\beta$  axis we find clustering of amplitude along a vertical located almost at the same position as the “bouncing ball” scar of the  $7442\text{Hz}$  wave pattern. As we move further to the left, the excitation amplitude decays, with the first bright fringe barely resolved.

The broken symmetry of the excited wave patterns we observe clearly indicates that they are not pure modes of the underlying unperturbed plate. In the 7-8 KHz range the experimental  $Q$ -factors, measured as the ratio of the resonance peak position to the 3dB width of the resonance peak, are between 50 and 90. This corresponds approximately to a minimum 75Hz level spacing that we can resolve experimentally. The observed resonance spacing in this frequency range is 200Hz which compares well with the mean Weyl level spacing for this plate of 300Hz. With such quality factors in the experiment we can conclude

that at each excitation frequency two-to-three pure modes of the system are excited.

The 2nd Newton's law written for small amplitude flexural vibration of a thin plate and the general form of the solution have the following form:

$$-D\Delta^2\psi + F_{dephase} + F_{dr} = \rho\partial_{tt}\psi \quad (1)$$

$$\psi(\mathbf{r}, t; f) = \sum_n \{\alpha_n \cos(2\pi ft + \gamma)\phi_n(\mathbf{r}) + \beta_n \sin(2\pi ft + \gamma)\phi_n(\mathbf{r})\} \quad (2)$$

$D$  is the flexural rigidity of the plate and  $\rho$  is the mass per unit area of the plate.  $F_{dephase}$  and  $F_{dr}$  are dephasing and driving forces respectively.  $f$  is the excitation frequency and  $\gamma$  is a fixed time-independent phase shift. The driving force in our experiment is harmonic and is localized at the position where the speaker needle is glued to the plate. In the absence of dephasing (with a proper choice of  $\gamma$ )  $\alpha_n = \delta(f - f_n)$  and  $\beta_n = 0$ . With a dephasing damping force both elastic and inelastic response is present and  $\alpha_n, \beta_n$  are frequency dependent coefficients. In this experiment damping occurs via plate-speaker and plate-air coupling, the former being the primary damping mechanism. Below, we write down expressions for imaged resonant wave patterns in terms of pure modes of the system and argue that these are also scarred.

The localization of wave pattern on the right at 7622 Hz excitation strongly suggests that we excite two closely spaced symmetry related modes:  $\phi_{i+1}^{-+}$  and  $\phi_{i+1}^{--}$ , with the first (second) sign in the superscript indicating odd (even) symmetry with respect to  $\alpha$  ( $\beta$ ) axis. The  $\phi_{i+1}^{-+}$  and  $\phi_{i+1}^{--}$  narrowly split mode pair located near 7622Hz and the  $\phi_i$  mode slightly lower than 7442Hz are marked on the level diagram in figure 3. The opposite symmetry of the two  $\phi_{i+1}$  modes with respect to  $\beta$  axis is needed to produce the observed localization. The odd symmetry with respect to the  $\alpha$  axis of  $\phi_{i+1}^{-+}$  and  $\phi_{i+1}^{--}$  is supported by the observed narrowness of the nodal line that runs along the  $\alpha$  axis, clearly passing through the right semi-disk center (cf. fig. 2). For even symmetry one would expect a wider bright white region reflecting a wider interval of small excitation amplitudes. A much wider bright region is always seen near the clamped edges where the derivative vanishes (cf. fig 1 and 2) and the amplitude increases slower from zero than near the  $\alpha$  axis of the 7622Hz excitation pattern. The placement of  $\phi_{i+1}^{-+}$  mode on the level diagram higher than  $\phi_{i+1}^{--}$  mode is motivated by a similar consideration. The odd-even mode picks up extra strain energy compared to the odd-odd mode along the symmetry line where its curvature is non-zero.

With the level diagram of figure 3, the three mode expansion of the wave pattern excited at 7622Hz has the following form:

$$\begin{aligned} \psi(7622) = & \sin(2\pi f_{exc}t) \{\beta_{i+1}^{-+}\phi_{i+1}^{-+} + \beta_{i+1}^{--}\phi_{i+1}^{--} + \beta_i\phi_i\} + \\ & \cos(2\pi f_{exc}t) \{\alpha_i\phi_i + \alpha_{i+1}^{-+}\phi_{i+1}^{-+} + \alpha_{i+1}^{--}\phi_{i+1}^{--}\} \end{aligned}$$

Since the two symmetry related modes are closely spaced with a spacing much smaller than the mean level spacing,  $\beta_{i+1}^{-+} \approx \beta_{i+1}^{--}$  and with  $\beta_i \ll \alpha_i \approx \alpha_{i+1} \ll \beta_{i+1}$  at 7622Hz, the excited wave pattern can be simplified to:

$$\psi(7622) = \sin(2\pi f_{exc}t) \{\beta_{i+1}\phi_{i+1}^R\} + \cos(2\pi f_{exc}t) \{\alpha_i\phi_i + \alpha_{i+1}\phi_{i+1}^R\} \quad (3)$$

where  $\phi_{i+1}^R$  is the sum(difference) of the two symmetry related modes with the sign chosen so to produce a wave pattern localized on the right side of the plate as is seen in the experiment. With the main contribution to this wave pattern localized on the right we

expect to find the signature of the pure  $i$ th mode of the plate on the left. This we believe is the origin of the amplitude clustering along the vertical just off to the left of the  $\beta$  symmetry axis.

Similarly, we can now write the wave pattern excited at 7442Hz as :

$$\psi(7442) = \sin(2\pi f_{exc}t)\{\beta_i\phi_i\} + \cos(2\pi f_{exc}t)\{\alpha_{i+1}\phi_{i+1}^R + \alpha_i\phi_i\} \quad (4)$$

The perturbing term is fully localized on the right hand side of the plate. We than expect to find a signature of the  $i$ th mode of an unperturbed plate to the left of the  $\beta$  symmetry axis and a wave pattern arising due to superposition of the  $i$ th and the  $(i + 1)st$  doublet on the right. Indeed, this is what we observe. The left side of the pattern in figure 1a is scarred by a “bouncing ball” orbit, while the right side exhibits no visible scarring, or regularity.

In an earlier work by Sridhar and Heller a localization effect similar to ours has been observed [9]. In that work resonant wave patterns of a MW cavity slightly perturbed from Sinai billiard shape were studied. There the authors of [9] were able to mix closely spaced symmetry related scarred modes of a Sinai shaped MW cavity, by slightly displacing the disk scatterer in the middle of the plate, with localization occurring on the side away from the displacement. When the symmetry of the cavity was reestablished the two mixed modes were split again. In our experiment we did not attempt to resolve individual symmetry related modes due to relatively low Q-factors of the excitation system.

To understand the scarring observed in high order modes within the simplest version of the PO formalism, we assume that the time-independent part of the solution along the scarred trajectories has a form  $u = A_\Gamma e^{iS_\Gamma}$ , where  $A_\Gamma$  is assumed to be a single valued function of position and is assumed to be nearly constant in the neighborhood of a classical trajectory  $\Gamma$ [18].  $S_\Gamma(q_\perp, q_\parallel)$  is a multivalued function written in terms of local coordinates  $q_\perp$  and  $q_\parallel$ , along and perpendicular to the trajectory.

In the high frequency limit the form of  $S_\Gamma(q_\perp, q_\parallel)$  is restricted. Far from the boundaries, sources, and caustics,  $S_\Gamma$  is nearly linear in both  $q_\perp$  and  $q_\parallel$ . Moreover,  $S_\Gamma$  is a rapidly growing function of  $q_\perp$  and  $q_\parallel$  in the limit of high order modes. In the regime where  $S_\Gamma(q_\perp, q_\parallel)$  is nearly linear, it is well described by an eikonal equation for a thin plate:

$$(\nabla S_\Gamma)^4 = \frac{12\rho(1 - \sigma^2)}{Eh^2}\omega_0^2, \quad (5)$$

where  $\omega_0$  denotes the frequency of the orbit. Unlike the eikonal equation for an ideal membrane, Eq. (6) is only valid up to frequencies for which volume deformations become appreciable, i.e., such that  $\frac{\Delta^2 u(\mathbf{r})}{\lambda^3} \sim \frac{h^3}{\lambda^3} \sim 1$ , where  $u(\mathbf{r})$  is the amplitude function for the mode and  $\lambda$  is the effective wavelength. At such short wavelengths and high frequencies the biharmonic wave equation itself breaks down. For the experimental results reported here we never reach this regime because  $\frac{h^3}{\lambda^3} \sim 10^{-3} \ll 1$ .

It can be seen that there are two types of solution of Eq. (6).  $S_\Gamma$  is either a real or complex function of position. Real  $S_\Gamma$  gives rise to propagating wave solutions which are plane wave-like in a homogeneous plate, exactly as for a membrane. Complex  $S_\Gamma$  yields exponentially decaying, or rising solutions of the wave equation. Each mode of the plate must be bounded, and hence the exponentially growing solutions cannot be present far

from the boundary. On the other hand, the decaying solutions decay to zero for distances significantly larger than a wavelength. This can be seen already in the one-dimensional clamped rod problem which serves as a useful guide in understanding various aspects of the two-dimensional plate [20,22].

It is straightforward to show that a plane wave propagating in a thin plate incident at an angle  $\alpha$  with respect to the normal onto a clamped plate edge, is reflected with a phase shift given by:

$$\delta = -2 \arccos \left( \sqrt{\frac{1 + \sin^2 \alpha}{2}} \right). \quad (6)$$

This expression can be obtained in the standard way by matching incoming and outgoing plane wave solutions under the condition that the wavelength is much smaller than the local boundary curvature [18]. Then, a simple quantization condition may be written for a trajectory  $\Gamma$  with  $N$  boundary reflections in the form:

$$k_{\parallel} L - 2 \sum_{i=1}^N \arccos \left( \sqrt{\frac{1 + \sin^2 \alpha_i}{2}} \right) = 2\pi n, \quad (7)$$

where  $k_{\parallel}$  is a wavevector component along the periodic trajectory,  $L$  is the total orbit length, and  $n$  is an integer “quantum” number.

For the 7442 Hz mode, the primary orbit of interest is the “bouncing ball” one. The amplitude build-up along the “bouncing ball” orbit in Fig. 1 (a) is clearly evident, and, by inspection, we expect the quantum number associated with this orbit to be  $n = 7$ . Substituting this into Eq. (8) along with the appropriate  $\alpha$  values for the orbit (i.e.,  $\alpha_1 = \alpha_2 = 0$ ), we obtain  $k_{\parallel} = 295 \text{ m}^{-1}$ . Then, we may use Eq. (1) to estimate a frequency contribution of  $f_{\parallel} = 6675 \text{ Hz}$ . Of course, the total frequency depends on  $k_{\parallel}^2 + k_{\perp}^2$ , so we use the difference of the observed  $f$  and calculated  $f_{\parallel}$  to estimate an effective  $k_{\perp} = 100 \text{ m}^{-1}$ . This corresponds to an effective “perpendicular” wavelength of  $\lambda_{\perp} = 6.30 \text{ cm}$ , which is comparable to the full width of the straight section of the plate. This observation is consistent with numerical studies of the Helmholtz equation, in which wavefunction scars of “bouncing ball” trajectories have an effective perpendicular wavelength which is slightly less than the full width of the straight section of the stadium boundary [1].

For the rectangular orbit that scars the 7622 Hz mode, there are four bounces each with  $\alpha_i = \pi/4$ . Using a quantum number of  $n = 16$ , we determine that  $k_{\parallel} = 271 \text{ m}^{-1}$  and  $f_{\parallel} = 5644 \text{ Hz}$ , considerably less than the measured frequency. In this case, the estimated perpendicular wavelength is rather small,  $\lambda_{\perp} = 3.90 \text{ cm}$ . This can be understood with the following argument. First, we note that the amplitude maxima of the rectangular orbit along the top straight edge of the plate should occur very near to the classical trajectory which lies a distance  $R(1 - \frac{1}{\sqrt{2}}) = 1.17 \text{ cm}$  below the plate edge in Fig. 2. Next, we consider the related problem of a long rectangular strip of plate which is clamped on one side and simply-supported on the other side (i.e., the amplitude and its second normal derivative vanish). Furthermore, the width  $l$  of the strip is selected such that the amplitude maximum of the lowest order vibrational mode occurs along the scarring orbit. This problem is easily solved using standard methods [20, 22], and we find  $l = 2.02 \text{ cm}$ . We expect that the length

$l$  should be close to the above estimate based on the quantization condition for one-half of the perpendicular wavelength,  $\lambda_{\perp}/2$ . We find  $\lambda_{\perp}/2 = 1.95$  cm, in good agreement.

We have observed qualitatively similar scarring effects in clamped metal plates that have non-stadium boundary shapes, but which are predicted to be chaotic for the Helmholtz equation, e.g., one-quarter of a “bow-tie” shape [24]. We also studied the spatial properties of vibrational modes in clamped plates with a circular boundary; in this case no significant scarring was found. We attempted to measure spectral statistics, but the present experimental set-up is not suitable for obtaining accurate results. The point driving source does not allow detection of those modes with nodal lines close to the driving point. Furthermore, if one moves the driving point to another location the eigenfrequencies shift due to coupling between the plate and the driving rod [8,24], so that one cannot combine spectra taken for different drive positions in any analysis of spectral statistics.

We have presented direct experimental evidence for scarring in the vibrational modes of a thin metal plate in the shape of a stadium. We have also introduced a novel quantization condition which is useful for estimating the experimental resonant frequencies of those modes that correspond to unstable periodic orbits of the underlying classical billiard system. It seems remarkable that scarring effects - predicted on the basis of semiclassical theories that include no frictional terms whatever - are clearly visible in this relatively low  $Q$  system. Further, it is surprising that of the three wave patterns we have imaged two were scarred by short periodic orbits. The imaging was done only at those excitation frequencies where the response of the plate was especially strong, since at the lower amplitudes the quality of interferograms is poor. At the 7442Hz and especially at 7622Hz excitation frequency one could actually hear the response of the plate. The  $Q$ -factors at these excitation frequencies were also largest detected. It is possible that due to reduced overlap between scarred and neighboring non-scarred modes the leakage of energy is suppressed and the  $Q$ -factors are enhanced. If true, such an effect would be generic for wave systems exhibiting scarring, with relatively small, but non-negligible losses. Further experiments on bimorph quartz piezoelectric plates which would allow a better coupling scheme are being planned to explore this possibility and to improve on already existing measurements.

We thank Prof. K. Matveev for helpful discussions, and thank Lester Chen, Dean Moyar, and Thomas Hund for help with the experimental set-up.

## REFERENCES

- [1] E. J. Heller, Phys. Rev. Lett., **53**, 1515 (1984).
- [2] E. B. Bogomolny, Physica D, **31**,169 (1988).
- [3] H.-J. Stöckmann and J. Stein , Phys. Lett. **64**, 2215 (1990).
- [4] S. Sridhar, Phys. Rev. Lett. **67**, 785 (1991).
- [5] J. Stein and H.-J. Stöckmann, Phys. Lett. **68**, 2867 (1992).
- [6] R. Blumel, I. H. Davidson, W. P. Reinhardt, H. Lin, and M. Sharnoff, Phys. Rev. A **45**, 2641 (1992).
- [7] P. A. Chinnery and V. F. Humphrey, Phys. Rev. E **53**, 272 (1996).
- [8] S. W. Teitsworth, to appear in *Proceedings of the 16th Sitges Conference* (Springer, Berlin, 1999).
- [9] S. Sridhar, E.J. Heller, Phys. Rev. E **46**, 1728, 1992
- [10] M. V. Berry, Proc. R. Soc. London, Ser. A, **413**, 183 (1987).
- [11] R. Weaver, J. Acoust. Soc. Am. **85**, 1005 (1989).
- [12] O. Bohigas, O. Legrand, C. Schmit, D. Sornette, J. Acoust. Soc. Am. **89**, 1456 (1991).
- [13] D. Delande, D. Sornette, R. Weaver, J. Acoust. Soc. Am. **96**, 1873 (1994).
- [14] C. Ellegard, T. Guhr, K. Lindemann, H. Q. Lorensen, J. Nygaard, and M. Oxborrow, Phys. Rev. Lett. **75**, 1546 (1995).
- [15] S. Deus, P. Koch, and L. Sirko, Phys. Rev. E, **52**, 1146 (1995).
- [16] H. Alt *et al.*, Phys. Rev. E **54**, 2303 (1996).
- [17] U. Dorr, H.-J. Stockmann, M. Barth, and U. Kuhl, Phys. Rev. Lett. **75**, 1030 (1998).
- [18] O. Legrand, C. Schmitt, D. Sornette, Eurorophys. Lett. **18**, 101 (1992).
- [19] E. Bogomolny and E. Hughes, Phys. Rev. E **57**, 5404 (1998).
- [20] Charles M. Vest, *Holographic interferometry* (Wiley, New York, 1979).
- [21] L. D. Landau and E. M. Lifshitz, *Theory of Elasticity*, 2nd ed. (Pergammon, London, 1970).
- [22] Philip M. Morse and K. U. Ingard, *Theoretical Acoustics*, (Princeton University Press, Princeton, 1986).
- [23] A. Starobin, undergraduate thesis, Duke University (1997).
- [24] A. Starobin and S. Teitsworth, unpublished (1997).
- [25] T. M. Antonsen, E. Ott, Q. Chen, and R. N. Oerter, Phys. Rev. E **51**, 111 (1995).

## FIGURES

FIG. 1. (a) Holographic interferogram for the 7442 Hz mode. The white dashed line superimposed on the hologram is a guide to the eye. (b) Plate schematic.  $\alpha$  and  $\beta$  are the symmetry axis.  $R_s$  is the position where the speaker needle was glued to the plate

FIG. 2. Holographic interferogram for the 7622 Hz mode. A rectangular orbit is superimposed on the right half of the image as a guide to the eye.

FIG. 3. the proposed level diagram of an underlying pure system unperturbed by the speaker-plate coupling and air damping. Each mode of an unperturbed plate is marked by the orbit that scars it.  $(-/+)$  notation is used to show the symmetry class of a given mode. The first index shows the symmetry with respect to the  $\alpha$  axis, the second with respect to the  $\beta$  axis. Minus sign stands for odd symmetry, plus for even.

This figure "figure1.jpg" is available in "jpg" format from:

<http://arxiv.org/ps/nlin/0010028v2>

This figure "figure2.jpg" is available in "jpg" format from:

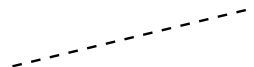
<http://arxiv.org/ps/nlin/0010028v2>

$f$  ↑

$i+1, (-+)$

$i+1, (--)$

7622Hz

$i$    7442 Hz